

M ultidimensional SUGRA Likelihood M aps

B .C .A llanach

DAMTP , CMS , Wilberforce Road, Cambridge, CB3 0WA , UK

C .G . Lester

Cambridge Laboratory. Madingley Road. Cambridge CB3 0HE , UK

Abstract : We calculate the likelihood map in the full 7 dimensional parameter space of the minimal supersymmetric standard model (MSSM) assuming universal boundary conditions on the supersymmetry breaking terms. Simultaneous variations of $m_0, A_0, M_{1=2}, \tan\beta, m_t, m_b$ and $m_s (M_Z)$ are applied using a Markov chain Monte Carlo algorithm. We use measurements of $b \rightarrow s (g-2)$ and $D_M h^2$ in order to constrain the model. We present likelihood distributions for some of the sparticle masses, the branching ratio of $B_s^0 \rightarrow \ell^+ \ell^-$ as well as $m_{\tilde{t}} - m_{\tilde{b}}$. The mass ordering allows the important cascade decay $\tilde{t}_1 \rightarrow \tilde{b}_1 \tilde{\chi}_1^0 \rightarrow \tilde{\chi}_1^0 \tilde{\chi}_1^0$ with a likelihood of 19.5%. Excluding the focus point scenario, the pseudoscalar Higgs funnel region has a likelihood of 43.4%, the stau coannihilation region has 24.6% and the light Higgs pole region has 3.1%.

Keywords: Dark Matter, Beyond Standard Model, Cosmology, MSSM , CMSSM , universality.

Contents

1. Introduction	1
2. MCMC Algorithm	4
2.1 Implementation	5
2.2 Convergence	8
3. Likelihood Maps	10
4. Theoretical Uncertainty	16
5. Conclusions	17
A. Toy Models and Sampling	19

1. Introduction

Weak-scale supersymmetry provides a well-documented solution to the technical hierarchy problem [1], which is particularly difficult to solve in a perturbatively calculable model. Specialising to a minimal extension of the Standard Model, the MSSM, one can provide a weakly interacting massive particle dark matter candidate, provided R-parity is respected by the model. Two examples of dark matter candidates are the gravitino [2] and the lightest neutralino [3], which are the subject of much recent investigation. The general MSSM is rather complicated due to the large number of free parameters in the supersymmetric (SUSY) breaking sector. However, the observed rareness of flavour changing neutral currents (FCNCs) suggests that the vast majority of parameter space for general SUSY breaking terms is ruled out. Particular patterns of SUSY breaking parameters can predict small enough FCNCs: for instance flavour universality. One highly studied subset of such terms is that of mSUGRA, often called the Constrained Minimal Supersymmetric Standard Model (CMSSM). In mSUGRA, at some high energy scale (typically taken to be the scale of unification of electroweak gauge couplings), all of the SUSY breaking scalar masses terms are assumed to be equal to m_0 , the scalar trilinear terms are set to A_0 and the gaugino masses are set equal (M_{1-2}). These are indeed strong assumptions, but they have several advantages for phenomenological analysis as the number of independent SUSY breaking parameters is much reduced. Indeed, assuming that the MSSM is the

correct model, the initial data from the Large Hadron Collider are likely to contain only a few relevant observables and so one may be able to test against a simple SUSY breaking model as an example [4]. As the data becomes more accurate and additional relevant observables are measured, the lack of a good fit would propel extensions of the simple model. One may then start to consider patterns of non-universality, for instance. For the rest of this paper though, given the lack of data to the contrary, we will assume mSUGRA. Aside from the universal soft term $m_0; A_0; M_{1-2}$, other non-standard model mSUGRA input parameters are taken to be $\tan\beta$, the ratio of the two Higgs vacuum expectation values, and the sign of μ (a parameter that appears in the Higgs potential of the MSSM).

When combined with large scale structure data, the Wilkinson microwave anisotropy probe (WMAP) [5, 6] has placed stringent constraints upon the dark matter relic density $\Omega_M h^2$. A common assumption, which we will adhere to here, is that the neutralino makes up the entire cold dark matter relic density. The prediction of the relic density of dark matter in the MSSM depends crucially upon annihilation cross-sections, since in the early universe SUSY particles will annihilate in the thermal bath. mSUGRA requires at least one of the following annihilation channels in order to be compatible with the WMAP constraint [7]:

Stau ($\tilde{\tau}$) co-annihilation [8] at small $\tan\beta$ where the lightest stau is quasi-degenerate with the lightest neutralino ($\tilde{\chi}_1^0$).

Pseudoscalar Higgs (A^0) funnel region at large $\tan\beta > 45$ where two neutralinos annihilate through an s-channel A^0 resonance [9, 10].

Light CP-even Higgs (h^0) region at low M_{1-2} where two neutralinos annihilate through an s-channel h^0 resonance [9, 11].

Focus point [12, 13, 14] at large m_0 where a significant Higgsino component leads to efficient neutralino annihilation into gauge boson pairs.

Several authors [15, 16, 17, 18, 19, 20, 21] have asked how the annihilation cross-section can be constrained by collider measurements in order to provide a more solid prediction of the relic density. This would then be fed into a cosmological model in order to predict $\Omega_M h^2$ for comparison with the value derived from cosmological observation, allowing a test of cosmological assumptions (and the assumption that there is only one component of cold dark matter). Of course, colliders could not unambiguously identify the lightest observed SUSY particle as the dark matter since it could always decay unobserved outside the detector. It would therefore be interesting to combine collider information with that derived from a possible future direct detection [22] of dark matter, providing corroboration and additional empirical information. Before such observations are made, however, we may ask how well current data constrains models of new physics.

This question has been addressed many times for m SUGRA by using the dark matter constraint. Most of the analyses (see, for example [23, 24, 25, 26, 27, 28, 29, 30]) x all but two parameters and examine constraints upon the remaining 2 dimensional (2d) slice of parameter space. The dark matter relic density constraint is the most limiting, but the branching ratio of the decay $b \rightarrow s$ and the anomalous magnetic moment of the muon ($g - 2$) also rule part of the parameter space out. Recent upper bounds from the Tevatron experiments on the branching ratio B_s [31] have the potential to restrict m SUGRA in the future, but the analysis of ref. [32] shows that the resulting constraints currently subsumed within other constraints. In the above analyses, limits are typically imposed separately, each to some prescribed confidence level. Such analyses have the advantage of being quite transparent: it is fairly easy to see which constraint rules out which part of parameter space. However, they have the disadvantages of not properly describing the combination of likelihoods coming from different experimental constraints and of having to assume ad hoc values for several input parameters. In particular, as well as the soft SUSY breaking input parameters, the bottom mass m_b , the strong structure constant $s(M_Z)$ and the top mass m_t can all have a strong effect on m SUGRA predictions. A large random scan of a four diagonal MSSM space involving 10^5 points that pass various prescribed constraints was presented in ref. [33], however the sampling of the 20d parameter space was necessarily sparse. The analysis is also subject to the limitation that likelihoods have not been combined; instead the measurements have been used as cuts to discard points. In ref. [34], the likelihood from the observables is calculated, properly combining different constraints, but again 1d and 2d slices through parameter space were taken. Of course the time taken to efficiently sample from a likelihood distribution using the naive method (a scan) scales like a power law with respect to the number of parameters, meaning that in practice even a high resolution 3d scan is difficult. By parameterising lines in 2d that are consistent with the WMAP dark matter constraint and scanning in two other parameters, the analysis of ref. [35] calculates the χ^2 statistic for the 2d part of a 3d parameter space which is consistent with the WMAP constraint on the dark matter relic density. The predicted value of $D_M h^2$ is not combined in the χ^2 with the other observables for this analysis, and the parameter $\tan \beta$ must be fixed. As the authors note [35], parts of the scan were sparse. In Ref. [36], a scan was performed which included variations of A_0 and $\tan \beta$ as well as other m SUGRA parameters. It is clear from this paper that the WMAP allowed region (expressed in the $M_{1=2} - m_0$ plane) becomes much larger from the A_0 variations. No likelihood distribution was given.

Baltz and Gondolo [37] demonstrated that a Markov chain Monte Carlo (MCMC) algorithm efficiently samples from the m SUGRA parameter space, rendering 4d scans in $m_0, A_0, M_{1=2}, \tan \beta$ feasible. However, they were interested in which parts of parameter space are compatible with the WMAP measurement of $D_M h^2$ and what the prospects are for direct detection there, not in the likelihood distribution. In

order to increase the efficiency of their parameter sampling, they changed the simple "Metropolis-Hastings" MCMC algorithm in order to achieve a better efficiency. As the authors state in their conclusions, this has the consequence that caution must be exercised when trying to interpret their results as a likelihood distribution. Indeed, we will show in a toy model that changes to the MCMC algorithm like the ones that Baltz and Gondolo made can alter the sampling from a distribution.

It is our purpose here to utilise the MCMC algorithm in such a way as to reliably calculate the combined likelihood of mSUGRA in the full dimensionality of its parameter space, thereby extending the previous studies. We will then be able to infer what is known about the multi-dimensional parameter space, including important variations of the SM quantities. These results will have implications for collider searches, for rare decays and for the dominant neutralino annihilation mechanism in the early universe.

In section 2, we briefly review the MCMC algorithm. We present the implementation used in the present paper to calculate the likelihood maps of mSUGRA parameter space and then demonstrate that the results are convergent using a particular statistical test. In section 3, we present the likelihood distributions and derived quantities of the 7d mSUGRA parameter space. In section 4, we illustrate the effects of theoretical uncertainties in the sparticle spectrum calculation and in section 5, we provide a summary and conclusions. In appendix A, we demonstrate with two different toy models that the algorithm used by Baltz and Gondolo may not provide a sampling proportional to the likelihood of the parameter space.

2. MCMC Algorithm

We now briefly review the Metropolis MCMC algorithm, but for a more thorough explanation, see refs. [37, 38]. Other adaptive scanning algorithms have recently been suggested in the context of high energy physics [39, 40] but (although they can be very useful for other purposes) they do not yield a likelihood distribution. A Markov chain consists of a list of parameter points ($x^{(t)}$) and associated likelihoods ($L^{(t)} = L(x^{(t)})$). Here t labels the link number in the chain. Given some point at the end of the Markov chain ($x^{(t)}$), the Metropolis-Hastings algorithm involves randomly picking another potential point ($x^{(t+1)}$) (typically in the vicinity of $x^{(t)}$) using some proposal pdf $Q(x; x^{(t)})$. If $L^{(t+1)} > L^{(t)}$, the new point is appended onto the chain. Otherwise, the proposed point is accepted with probability $L^{(t+1)} / L^{(t)}$ and, if accepted, added to the end of the chain. If the point $x^{(t+1)}$ is not accepted, the point $x^{(t)}$ is copied on to the end of the chain instead.

Providing "detailed balance" is satisfied, it can be shown [38] that the sampling density of points in the chain is proportional to the target distribution (in this case, the likelihood) as the number of links goes to infinity. In the context of this analysis,

detailed balance states that for any two points x_a, x_b

$$Q(x_a; x_b)L(x_b) = Q(x_b; x_a)L(x_a); \quad (2.1)$$

i.e. the probability of sampling a point x_a from the likelihood distribution and then making a transition to x_b be equal to the probability of sampling x_b and making a transition to x_a .

The Metropolis-Hastings MCMC algorithm is typically much more efficient than a straightforward scan for $D > 3$; the number of required steps scales roughly linearly with D rather than as a power law. The sampling is in principle independent of the form of Q as $t \geq 1$ as long as it is bigger than zero everywhere. However, Q must be chosen with some care: since in practice we can only sample a finite number of points, the choice of the form of Q can determine whether the entire parameter space is sampled and how quickly convergence is reached.

Baltz and Gondolo used a geometrical model for Q : choosing a random distance from the point $x^{(t)}$ and using a direction that was calculated from the positions of previous points in the chain. The width of the random radius pdf was calculated depending upon previous points in the chain in order to increase the efficiency of the calculation, aiming to accept roughly 25% of potential points. Either of these changes upset detailed balance and may spoil the sampling. We demonstrate in particular in Appendix A with toy models that the width changing modification gives a sampling that is not proportional to the target density.

2.1 Implementation

in SUGRA is ruled out by negative results in sparticle searches for $m_0 < 60$ GeV or $M_{1=2} < 60$ GeV. $\tan\beta > 0$ is favoured by the measurement of the anomalous magnetic moment of the muon. On general naturalness grounds¹, we expect m_0 and $M_{1=2}$ to not be too large: less than say, 2 TeV. $\tan\beta$ is bounded from below by negative searches at LEP 2 for h^0 (and perturbativity of the top Yukawa coupling) and from above by perturbativity of the Yukawa couplings up to the unification scale. Here, we restrict the parameter space to that shown in Table 1.

Unfortunately, this automatically excludes the focus point region, which is at much higher values of m_0 than the range considered in Table 1. It has been argued that a quantitative measure of net-tuning in the focus point region is not too large [12, 13], however the net-tuning of the top quark Yukawa coupling is enormous [41]. The added volume of parameter space necessary to include the focus point region means that convergence is difficult to achieve with the CPU power available

parameter	range
$\text{sign}(\beta)$	+1
A_0	-2 TeV 2 TeV
m_0	60 GeV 2 TeV
$M_{1=2}$	60 GeV 2 TeV
$\tan\beta$	2 60

Table 1: Parameter ranges considered.

¹That is, to avoid a large cancellation between weak scale SUSY breaking terms in order to get a small value of $\tan\beta$.

to us. Also, focus point region points take much more time to accurately calculate the spectra for than other viable mSUGRA points. For now, we will simply neglect the focus point region for convenience.

$m_{\tilde{\chi}_1^0}$	37	$m_{\tilde{\chi}_1^1}$	67.7	$m_{\tilde{g}}$	195	$m_{\tilde{\tau}_1}$	76
$m_{\tilde{\chi}_2^0}$	88	$m_{\tilde{\chi}_2^1}$	86.4	$m_{\tilde{b}_1}$	91	$m_{\tilde{e}_R}$	250
$m_{\tilde{\tau}_e}$	43.1						

Table 2: Lower bounds applied to sparticle mass predictions in GeV.

We calculate the MSSM spectrum from mSUGRA parameters, by using the program SOFTSUSY1.9.2 [42]. Ideally we would like to include data from negative search results from collider data within a combined likelihood. Unfortunately it is difficult to obtain the data in such a form and so instead, we assign a zero likelihood to any point for which at least one of the constraints [43] in Table 2 is not satisfied. We also implement a parameterisation² of the 95% confidence level limits [45] on m_h ($g_{hZ} = g_{hZ}^{SM}$), where $g_{hZ} = g_{hZ}^{SM}$ is the ratio of the MSSM higgs coupling to two Z^0 bosons to the equivalent Standard Model coupling. In order to take a 3 GeV uncertainty on the mSUGRA prediction of m_h into account, we add 3 GeV [46, 44] to the m_{h^0} value that is used in the parameterisation. In the MSSM, $g_{hZ} = g_{hZ}^{SM} = \sin(\theta)$ and in practice, it is easier to apply limits in terms of the inverse parameterisation $\sin^2(\theta)(m_{h^0})$ as shown in Table 3.

m_{h^0} = GeV range	upper bound on $\sin^2(\theta)$
90–99	$-6.1979 + 0.12313 m_{h^0} - 0.00058411 (m_{h^0} = \text{GeV})^2$
99–104	$35.73 - 0.69747 m_{h^0} + 0.0034266 (m_{h^0} = \text{GeV})^2$
104–109.5	$21.379 - 0.403 m_{h^0} + 0.0019211 (m_{h^0} = \text{GeV})^2$
109.5–114.4	$1 / (60.081 - 0.51624 m_{h^0} = \text{GeV})$

Table 3: Parameterisation of 95% confidence level LEP 2 Higgs limits on the m_{h^0} – $\sin^2(\theta)$ plane. All points with $m_{h^0} < 90$ GeV are ruled out.

The spectrum is transferred via the SUSY Les Houches Accord [47] to the computer program micrOMEGAs1.3.5 [48, 49] in order to calculate several quantities used to calculate the likelihood of a parameter point. We will use six measurements in order to construct the total likelihood of any given point of parameter space. As mentioned in the introduction, we make the assumption that the neutralino makes up the entire cold dark matter relic density as constrained by WMAP:

$$D_M h^2 = 0.1126^{+0.0081}_{-0.0091} : \quad (2.2)$$

The anomalous magnetic moment of the muon has been measured [50] to be higher than the Standard Model prediction [51, 52]. The experimental measurement is so

²Developed by P. Slavich for Ref. [44].

precise that the comparison is limited by theoretical uncertainties in the Standard Model prediction. Following Ref. [53], we constrain any new physics contribution to be

$$\frac{(g-2)}{2} = 19.0 \pm 8.4 \cdot 10^{-10}; \quad (2.3)$$

Adding theoretical errors [54] to measurement errors [55] in quadrature for the branching ratio for the decay $b \rightarrow s$, one obtains the empirically derived constraint

$$BR(b \rightarrow s) = 3.52 \pm 0.42; \quad (2.4)$$

The Standard Model inputs' measurements also contribute to the likelihood. We take these to be [43], for the running bottom quark mass in the modified minimal subtraction scheme,

$$m_b(m_b)_{\overline{MS}} = 4.2 \pm 0.2 \text{ GeV}; \quad (2.5)$$

for the pole mass of the top quark [56],

$$m_t = 174.3 \pm 3.4 \text{ GeV}; \quad (2.6)$$

and for the strong coupling constant in the modified minimal subtraction scheme at M_Z

$$\alpha_s(M_Z)_{\overline{MS}} = 0.1187 \pm 0.002; \quad (2.7)$$

A prediction p_i of one of these quantities, where

$$i \in \{m_b(m_b)_{\overline{MS}}, m_t, \alpha_s(M_Z)_{\overline{MS}}, (g-2)_{\text{EM}}, BR(b \rightarrow s), h^2 g\} \quad (2.8)$$

with measurement $m_i - s_i$ yields a log likelihood

$$\ln L_i = -\frac{(m_i - p_i)^2}{2s_i^2} - \frac{1}{2} \ln(2\pi) - \ln s_i; \quad (2.9)$$

assuming the usual Gaussian errors. To form the combined likelihood, one takes $\ln L^{\text{tot}} = \sum_{i=1}^p \ln L_i$, corresponding to the combination of independent Gaussian likelihoods.

We assume that the proposal function is the product of Gaussian distributions along each dimension $k = 1, 2, \dots, D$ centred on the location of the current point along that dimension, i.e. $x_k^{(t)}$:

$$Q(x^{(t+1)}; x^{(t)}) = \prod_{k=1}^D \frac{1}{\sqrt{2\pi l_k}} e^{-(x_k^{(t+1)} - x_k^{(t)})^2 / 2l_k^2}; \quad (2.10)$$

where l_k denotes the width of the distribution along direction k . By trial and error we find that using values of l_k that are equal to the parameter range of dimension k given in Table 1 divided by 25 works well. For the Standard Model inputs, we choose $l_k = 8$ for $k=25$.

In order to start the chain we follow the following procedure, which finds a point at random in parameter space that is not a terrible fit to the data. We pick some $y^{(0)}$ at random in the mSUGRA parameter space using a flat distribution for its probability density function (pdf). The Markov chain for y is evolved a sufficient number of steps (t) such that $\ln L(y^{(t)}) > -5$, i.e. the initial chain has found a reasonable fit. We then set $x^{(0)} = y^{(t)}$, continuing the Markov chain in x and discarding the "burn-in" chain y . The reasonable fit point is typically found long before 2000 iterations of the Markov chain.

2.2 Convergence

In order that likelihood distributions calculated in this paper be considered reliable, it is important to check convergence of the MCMC. This is done by running 9 independent Markov chains, each with random starting positions as described above. The starting positions are chosen in the ranges presented in Table 1 with a flat pdf, since it is important for the convergence measure that the initial values be over distributed compared to the likelihood function one samples from. By examining the variance and means of input parameters within the chains and between the 9 different chains, we will construct a quantity [57] \hat{R} . \hat{R} will provide an upper bound on the factor of expected decrease of variance of 1d likelihood distributions if the chain were iterated to an infinite number of steps. An \hat{R} value can be constructed for scalar quantities that are associated with a point $x^{(t)}$.

The analysis of the \hat{R} convergence statistic follows Ref. [57] closely. We consider $c = 1, \dots, M$ chains ($M = 9$ here), each with $N = 10^6$ steps. Then we may define the average input parameter along direction k for the chain c and the average amongst the ensemble of chains

$$\bar{x}_k|_c = \frac{1}{N} \sum_{t=1}^{N^k} x_k^{(t)}|_c; \quad x_k = \frac{1}{M} \sum_{c=1}^M \bar{x}_k|_c; \quad (2.11)$$

respectively. The variance of chain c along direction k is

$$V_k|_c = \frac{1}{N} \sum_{t=1}^{N^k} (x_k^{(t)}|_c - \bar{x}_k|_c)^2; \quad (2.12)$$

so that we have the average of the variances within a chain

$$w_k = \frac{1}{M} \sum_{c=1}^M V_k|_c \quad (2.13)$$

and the variance between chains' averages

$$B_k = \frac{1}{M-1} \sum_{c=1}^M (x_k|_c - \bar{x}_k)^2; \quad (2.14)$$

The basic ratio constructed corresponds to

$$R_k = \frac{\frac{N-1}{N}w_k + B_k/N (1 + \frac{1}{M})}{w_k}; \quad (2.15)$$

As long as the initial seed parameters of the Markov chain are over-distributed, i.e. they have larger variance than the likelihood, this ratio will be larger than one [57] if the chains have not converged or if they have not had time to explore the entirety of the parameter space. It tends to one only if both of these conditions are met. In order to construct \hat{R}_k , we must take into account the sampling variability of $\langle x_k \rangle_c$ and $\langle N_k \rangle_c$. The variance of chain variances along direction k is estimated to be

$$v_k = \frac{1}{M-1} \sum_{c=1}^{M-1} (\langle N_k \rangle_c - w_k)^2; \quad (2.16)$$

and we must take into account the following estimates of co-variances between the values of $\langle x_k \rangle_c$ and $\langle N_k \rangle_c$:

$$\langle \cdot \rangle_1 = w_k x_k^2 + \frac{1}{M-1} \sum_{c=1}^{M-1} \langle N_k \rangle_c \langle x_k \rangle_c^2; \quad \langle \cdot \rangle_2 = w_k x_k + \frac{1}{M-1} \sum_{c=1}^{M-1} \langle N_k \rangle_c \langle x_k \rangle_c; \quad (2.17)$$

Defining the total estimated variance of the target distribution along direction k

$$V_k = \frac{1}{M} (1 - \frac{1}{N})^2 v_k + \frac{2(M+1)^2}{M(M-1)} (B_k/N)^2 + 2 \frac{(N-1)(M+1)}{M^2 N} (\langle \cdot \rangle_1 - 2x_k \langle \cdot \rangle_2); \quad (2.18)$$

where we have degrees of freedom

$$df_k = 2 \frac{R_k w_k + B_k/N (M-1)}{V_k}; \quad (2.19)$$

leading us to the main equation for the estimated reduction in the sampled variance as t! 1 :

$$\hat{R}_k = R_k \frac{df_k}{2}; \quad (2.20)$$

Here, we define $r = \max_k f \frac{p}{\hat{R}_k}$. Values of $r < 1.05$ are considered to signify convergence and compatibility of the chains, since we could only hope to decrease the scale of any of the input parameter distributions by at most 5% by performing further Markov Chain steps. In Fig. 1, we show the quantity r as a function of step number. $r < 1.05$ is met already for 500 000 steps indicating adequate convergence, although for the results we present below we always use the full 9 1 000 000 sample.

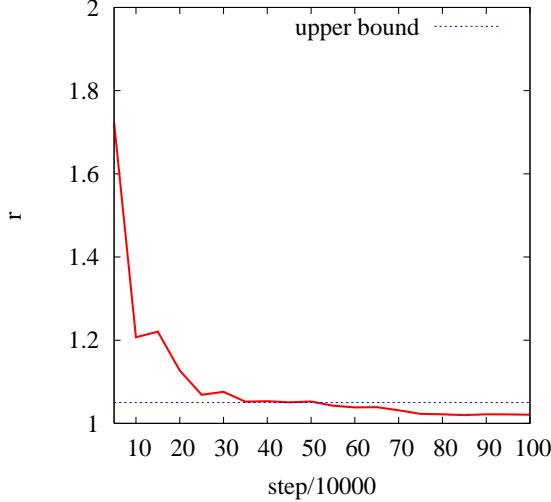


Figure 1: Estimate of potential scale reduction shown as a function of the number of Markov chain Monte Carlo steps. The upper bound we require for convergence is shown as a horizontal line.

3. Likelihood Maps

The number of input parameters exceeds the number of data and the likelihood shows a rough degeneracy along directions which give iso-lines of $\Delta M h^2$. The parameters of the best-fit point of the MCMC does not therefore supply us with much information, but the value of the likelihood at that point is interesting: a very small value would indicate a high χ^2 and therefore a bad fit. The best-fit point sampled by the MCMC with 7d input parameter space was

$$\begin{aligned} m_0 &= 938 \text{ GeV}; M_{1=2} = 336 \text{ GeV}; A_0 = 1364 \text{ GeV}; \tan \theta = 58.5; \\ m_b (m_b) &= 4.21 \text{ GeV}; m_t = 174.1 \text{ GeV}; s(M_Z) = 0.1190; \end{aligned} \quad (3.1)$$

leading to predictions of $(g-2)_e = 2.0 \times 10^{-9}$, $BR(b \bar{b} \rightarrow s \bar{s}) = 3.55 \times 10^{-4}$ and $\Delta M h^2 = 0.114$ and corresponding to a combined likelihood of $L = 0.97$. The point is within the A^0 pole region, and the high value of the likelihood gives us confidence that MUSGRA can fit well to current data.

We display binned sampled likelihood distributions in Figs. 2a-2f for the full m_t , $m_b (m_b)$, $s(M_Z)^{MS}$, m_0 , A_0 , $\tan \theta$ and $M_{1=2}$ parameter space. The unseen dimensions in each figure have been marginalised with flat priors in the ranges of parameters considered in Table 1. We have used 75-75 bins, normalising the likelihood in each bin to the maximum likelihood in any bin in each 2d plane.

In each plot, the h^0 pole s-channel resonant annihilation region is present close to the lowest values of $M_{1=2}$. It can be seen as a vertical sliver in the top-left hand corner of the m_0 vs $M_{1=2}$ as in Fig. 2a and the slim band ranging across the bottom of Figs. 2d, 2f. The region in Fig. 2a at low values of m_0 is primarily a co-annihilation

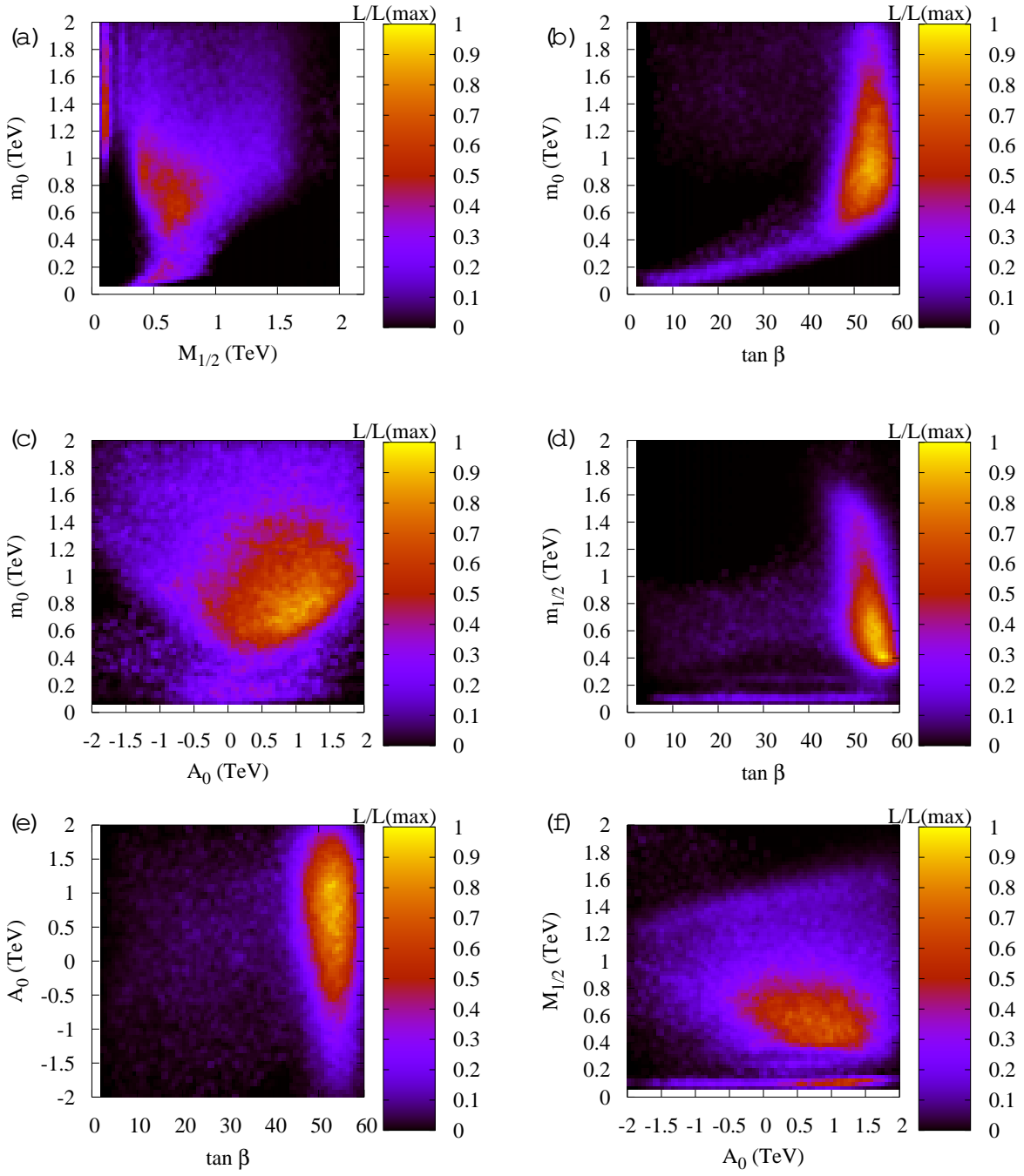


Figure 2: Likelihood maps of mSUGRA parameter space. The graphs show the likelihood distributions sampled from 7d parameter space and marginalised down to two. The likelihood (relative to the likelihood in the highest bin) is displayed by reference to the bar on the right hand side of each plot.

region where slepton-neutralino annihilation contributes significantly to the depletion of the neutralino relic density in the early universe. The pseudoscalar Higgs (A^0) s-channel annihilation channel occurs at high $\tan \beta = 50 - 60$ and in the intermediate

areas of $m_0 = 500 - 1600$ GeV, $M_{1=2} = 250 - 1400$ GeV. In the literature, the most common way to display M SUGRA results is to present them in 2d in the m_0 - $M_{1=2}$ plane, where thin strips are observed (see for example Ref. [35]) that are consistent with the WMAP constraint upon $D_M h^2$. Fig. 2a demonstrates (in corroboration with Refs. [37, 36]) that the strips are truly a result of picking a 2d hyper-surface in parameter space: if one performs a full multi-dimensional scan, there is a large region in the m_0 - $M_{1=2}$ that is consistent with the data. The bottom right hand side corner of Fig. 2a is ruled out primarily by the fact that the LSP is charged. Large $M_{1=2}$ is disfavoured by the (g_2) result. The bottom left-hand corner of Fig. 2a is ruled out by a combination of dark matter and direct search constraints. We see an interesting correlation between m_0 and $\tan\beta$ in Fig. 2b: the region extending to low $\tan\beta$ and m_0 is essentially the co-annihilation region.

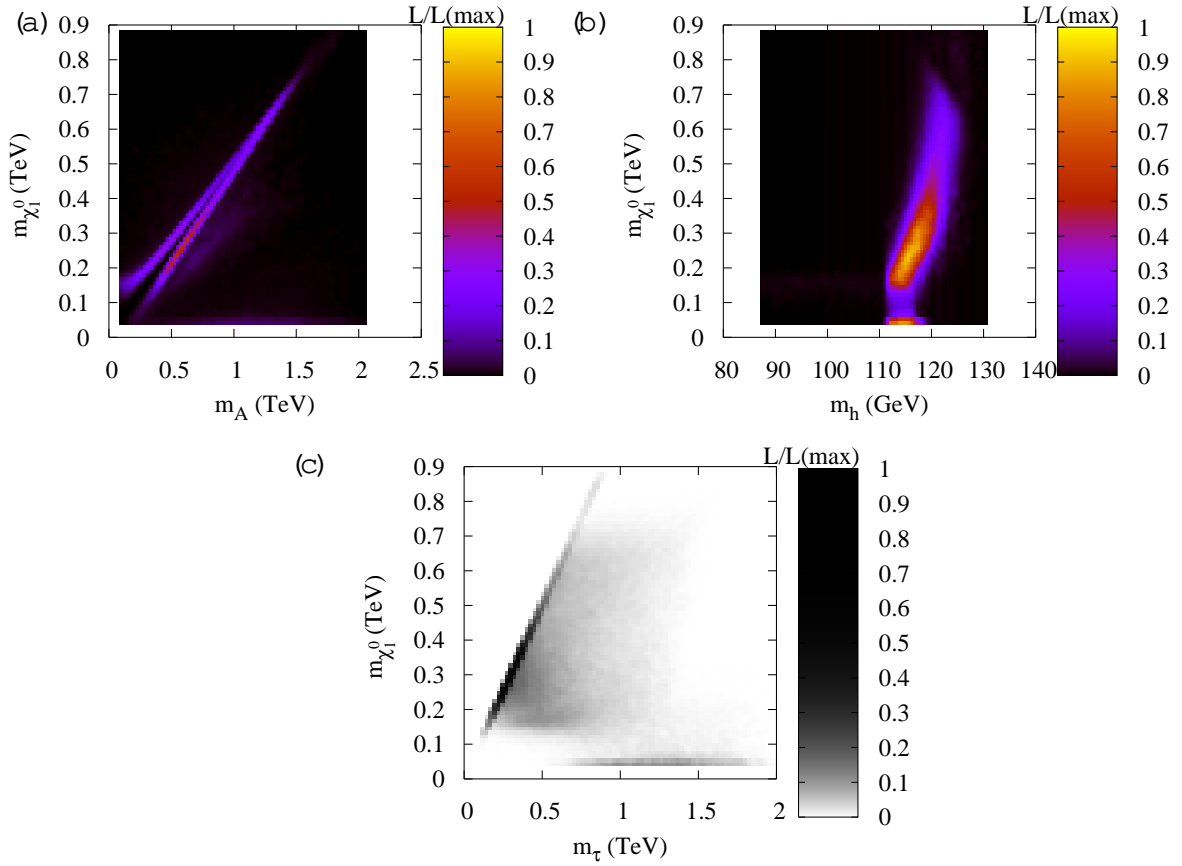


Figure 3: Likelihood distributions of masses in M SUGRA. The graphs show the likelihood distributions marginalised down to 2d. The likelihood (relative to the likelihood in the highest bin) is displayed by reference to the bar on the right hand side of each plot.

We display some binned likelihood distributions of M SSM particle masses in Figs. 3a-3c that are relevant for dark matter annihilation. In Fig. 3a, the A^0 -pole resonance region is clearly discernable: at just above a line $2m_1^0 = M_{A^0}$ and just

below it, there is just enough annihilation to produce the observed relic density. Throughout much of the parameter space ($M_A < 1 \text{ TeV}$), the exact resonance condition depletes the relic density $D_M h^2$ to be too small. At around $M_A = 1 \text{ TeV}$, exact resonance is required in order to sufficiently deplete the relic dark matter density. The rest of the likelihood density is spread over the dark part of the plot and is mostly too diffuse to be visible. In Fig. 3b, there are two detectable regions: the small one with the maximum 2d binned likelihood at the lowest possible values of $m_{\tilde{1}}$ corresponds to the h^0 -pole region. The larger upper high likelihood region is an amalgam of the co-annihilation and A^0 -pole regions. As a by-product we see that values of $m_h > 126 \text{ GeV}$ are disfavoured in the mSUGRA model. Finally, in Fig. 3c, the stau co-annihilation region is visible as the diagonal dark line and the h^0 -pole region as the lower likelihood horizontal dark line. The rest of the likelihood density is diffusely distributed in between these two extremes.

We show the sampled likelihood distribution for $\tilde{\chi}_1^0$, m_g , $m_{\tilde{1}}$ and $m_{\tilde{2}}$ in Fig. 4a. The likelihood distributions have been placed into 75 bins of widths that are equal for the different types of sparticles. They are each normalised to an integrated likelihood of 1. The spike at low values of the gluino mass corresponds to the h^0 -pole region of mSUGRA. This spike has a good chance of being covered at the Tevatron experiments before the LHC starts running [58]. It should be noted that upper limits upon the scalar sparticle masses inferred from Fig. 4a are due largely to the definition of the range of the initial parameters (m_0 being less than 2 TeV). Nevertheless, it is clear that there is already some preference from the combined data for various ranges of sparticle masses and upper bounds upon the gaugino masses. For example, values of $m_g > 3.5 \text{ TeV}$ and $m_g = 400 \text{ GeV} - 800 \text{ GeV}$ are disfavoured, as well as $m_{\tilde{2}} < 800 \text{ GeV}$. In Fig. 4b, the mass splitting between the lightest stau and lightest neutralino is shown. The inset in the figure displays the quasi-degenerate co-annihilation region at low mass splittings. The peaked region at $m_{\tilde{1}} = m_{\tilde{2}} < 10 \text{ GeV}$ is likely to be difficult to discern at the Large Hadron Collider (LHC). One would wish to measure decays of the lightest staus in order to check the co-annihilation region, but reconstructing a relevant soft $\tilde{\chi}_1^0$ resulting from such a decay is likely to prove problematic. On the other hand, a linear collider with sufficient energy to produce sparticles could provide the necessary information [59, 18]. The predicted likelihood distribution of the $B_s \rightarrow \pi^+ \pi^-$ branching ratio is shown in Fig. 4c. Possible values for this observable were found with a random scan of unconstrained MSSM parameter space in Ref. [60] (no likelihood distribution was given). The region to the right hand side of the vertical line is ruled out from the combined CDF/D0 95% C.L. exclusion [31]³ limit $B(R(B_s^0 \rightarrow \pi^+ \pi^-)) < 3.4 \cdot 10^{-7}$. We have not cut points violating this constraint, but this has negligible effect since there are only a small number of them. The 2d marginalisation of the branching ratio versus M_{1-2} shows a peak at

³There are newer CDF/D0 bounds [61], but no combination yet.

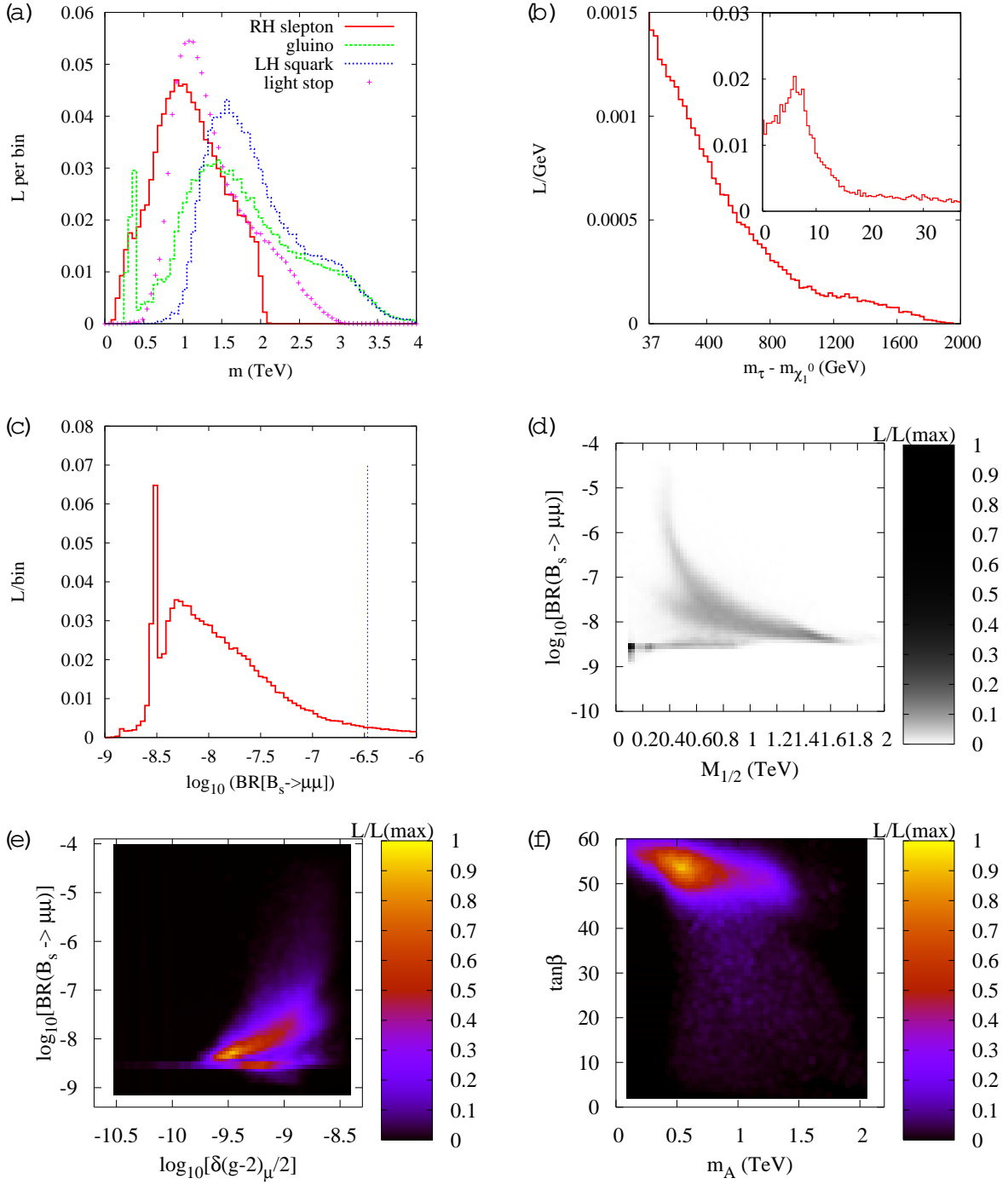


Figure 4: (a) Selected sparticle mass likelihood distributions in m SUGRA, (b) stau-neutralino mass difference likelihood distribution where the insert shows a blow-up of the quasimass-degenerate region. (c) branching ratio for the decay $B_s \rightarrow \mu\mu$. The Tevatron upper bound is displayed by a vertical line. (d) Likelihood density marginalised to the 2d plane $\text{BR}(B_s \rightarrow \mu\mu)$ versus $M_{1/2}$. (e) Correlation between $\text{BR}(B_s \rightarrow \mu\mu)$ and $(g-2)_\mu$. (f) Likelihood marginalised to the $\tan\beta$ - m_A plane.

very low $M_{1/2}$ values, as Fig. 4d displays. This indicates that the spike in Fig. 4c at branching ratios of about $10^{-8.6}$ is due to the h^0 -pole region. Lowering the empirical

upper bound on the $B_s \rightarrow \mu^+ \mu^-$ branching ratio will significantly cut into the allowed mSUGRA parameter space. A significant lowering of the bound upon this branching ratio is expected in the coming years from the Tevatron experiments and from LHCb. For example, it is estimated [58] that the Tevatron could exclude a branching ratio of more than 2×10^{-8} with 8 fb^{-1} of integrated luminosity. This corresponds to ruling out 32.9% of the currently allowed likelihood density. Predictions for $\text{BR}(B_s \rightarrow \mu^+ \mu^-)$ were correlated with those for $(g-2)_\mu$ in Ref. [62] in mSUGRA. For a given mSUGRA parameter point, a correlation was shown when $\tan \beta$ was varied. The authors conclude that for high $\tan \beta$, an enhancement of $\text{BR}(B_s \rightarrow \mu^+ \mu^-)$ is implied by the $(g-2)_\mu$ measurements. We re-examine this statement in view of the full dimensionality of the mSUGRA parameter space in Fig. 4e. The correlation is seen to be far from perfect, the likelihood distribution being highly smeared in terms of the two measurements. Nevertheless, there is a mild correlation between $\text{BR}(B_s \rightarrow \mu^+ \mu^-)$ and the SUSY contribution to $(g-2)_\mu$ at the highest likelihoods, as evidenced by the bright oblique stripe in Fig. 4e. In Fig. 4f, we show the likelihood distribution in the $\tan \beta - m_A$ plane. There is a significant amount of likelihood density towards the top left-hand side of the plot, where the Tevatron is expected to have sensitivity [58] (covering $\tan \beta > 40$ for $m_A < 240 \text{ GeV}$ for 8 fb^{-1} of integrated luminosity). LHC experiments should be able to observe the A^0 for the entire high likelihood range [4].

We now ask what are the likelihoods of the different regions of relic density depletion in mSUGRA parameter space. In order to sharply delineate the regions, we define them as follows: the co-annihilation region is defined such that $m_{\tilde{\chi}_1^0}$ is within 10% of $m_{\tilde{\chi}_2^0}$. The $h^0 = A^0$ -pole regions have $2m_{\tilde{\chi}_1^0}$ within 10% of m_{h^0} , m_{A^0} respectively.

The likelihoods of these regions are shown in Table 4. We estimate the uncertainty by calculating the standard deviation on the 9 independent Markov chain samples. The quoted error thus reflects an uncertainty due not to experimental errors, but to a finite simulation time of the Markov chain. We see that the h^0 -pole region has a relatively low likelihood whereas for the A^0 -pole and co-annihilation regions the likelihood is larger. These likelihoods do not add to a total of one for several reasons. Firstly, some of the points sampled will be a few sigma away from the $\text{DM } h^2$ constraint and may fall outside of our definitions of the individual regions. Also, since the full 7d parameter space does not provide a sharp distinction between the various regions, there will be some points for which several mechanisms significantly contribute to the relic density annihilation mechanism, but for which none of the criteria that we have set in order to pigeon-hole the point are quite satisfied. A better defined procedure might per-

Region	likelihood
h^0 pole	0.03 0.01
A^0 pole	0.43 0.04
co-annihilation	0.24 0.06

Table 4: Likelihood of being in a certain region of mSUGRA parameter space.

haps be to determine regions on the basis of the dominant annihilation mechanism, but since we are only looking for an rough indication of the region involved, the procedure adopted here will suffice⁴

As an aside, we note that the decay chain $q_L^+ \rightarrow \tilde{q}_2^0 \rightarrow \tilde{q}_1^0$ exists with a likelihood of 0.19 0.05 (this number is just based upon the mass ordering and does not take into account the branching ratio for the chain). The existence of such a chain allows the extraction of several functions of sparticle masses from kinematic endpoints and they have been used in many LHC analyses, for example Refs. [4, 63, 64].

4. Theoretical Uncertainty

Theoretical uncertainties in the sparticle mass predictions have been shown to produce non-negligible effects in fits to data [65], including fits to the relic density [20, 7, 66]. In this section, we perform a second MCMC analysis taking theoretical uncertainty into account in order to estimate the size of its effect. SOFTSUSY performs the Higgs potential minimisation then calculates sparticle pole masses at a scale $M_{\text{SUSY}} = \sqrt{m_{\tilde{q}_1} m_{\tilde{q}_2}}$. This scale is chosen because it is hoped that loop corrections to the pole mass corrections that are not yet taken into account (typically two-loop corrections) are small at this scale. In order to estimate the size of theoretical uncertainties, we vary this scale by a factor of two in either direction (but it is always constrained to be greater than M_Z)⁵. Implementation of the uncertainty in the MCMC algorithm is simple: we simply add an input parameter x which is bounded between 0.5 and 2, giving the factor by which M_{SUSY} is to be multiplied. The MCMC is then re-run as before and explores the full 8d parameter space (including x) accordingly.

Such a procedure automatically takes into account the correlations in predictions due to correlated theoretical uncertainties in the sparticle mass predictions. The likelihoods of the three mSUGRA regions are shown in Table 5. The likelihoods are approximately equal to those for the 7d case, as a comparison to Table 4 indicates. In fact, comparing results and plots produced with and without theoretical uncertainties, the results are generally very similar. This indicates that the theoretical uncertainties don't make a huge difference to the 1d and 2d marginalisations compared to those coming from the data. The decay chain $q_L^+ \rightarrow \tilde{q}_2^0 \rightarrow \tilde{q}_1^0$ has a likelihood of 0.25 0.06, not significantly higher than the case when theoretical uncertainties were not taken into account.

⁴We note that we find no evidence of a stop co-annihilation region, perhaps because of our chosen range of A_0 .

⁵A more complete estimate would be to calculate the Higgs potential minimisation conditions and the sparticle masses all at different scales, varying each independently by a factor of two. However, such a prescription is impractical here due to CPU time constraints.

Region	likelihood
h^0 pole	0.02 0.01
A^0 pole	0.41 0.06
co-annihilation	0.29 0.06

Table 5: Likelihood of being in a certain region of mSUGRA parameter space including theoretical uncertainties in the sparticle spectrum calculation.

Two of the 2d marginalised likelihoods change slightly when theoretical uncertainties are included and we present them in Figs. 5a,5b. Comparing with Fig. 2a, we see that Fig. 5a shows two main effects: the Higgs pole region at $m_0 = M_{1/2}$ becomes somewhat reduced in importance and the co-annihilation region dominates the likelihood over the Higgs pole region more. Fig. 5b also displays the enhanced low m_0 co-annihilation region when compared to Fig. 2c. Marginalising mass likelihood distributions down to 1d (as in Fig. 4a for example), one obtains distributions that are identical to the 7d case except for small statistical fluctuations.

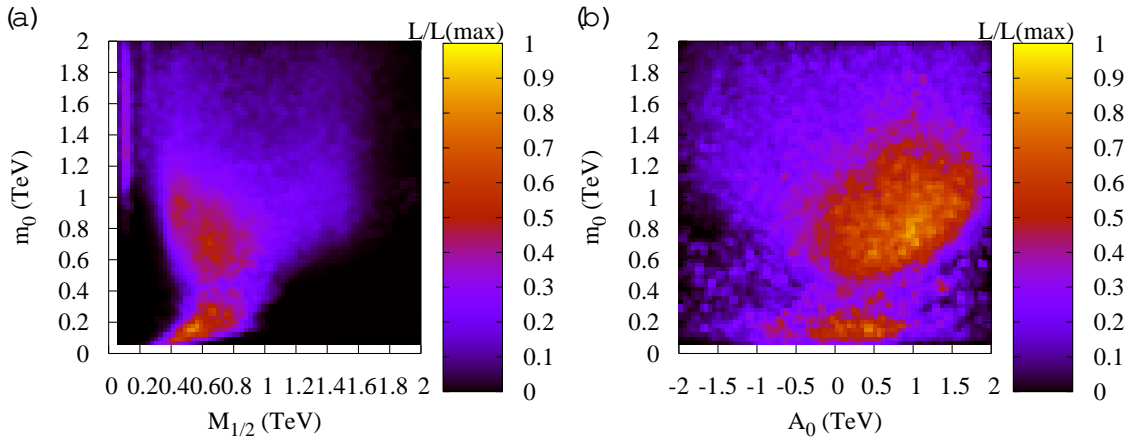


Figure 5: Likelihood maps of mSUGRA parameter space including theoretical uncertainty. The graphs show the likelihood distributions sampled from 8d parameter space and marginalised down to two. The likelihood (relative to the likelihood in the highest bin) is displayed by reference to the bar on the right hand side of each plot.

5. Conclusions

We have successfully employed an MCMC algorithm to provide likelihood maps of the full 7d input parameter space of mSUGRA. By using a statistical test, we have shown that the likelihood distributions have achieved good convergence before a total of $9 \cdot 10^6$ samplings of the likelihood. We have presented the likelihood marginalised down to each 2d mSUGRA parameter pair. Such plots provide the totality of the current information we have about the model given the experimental constraints. Theoretical uncertainties in the sparticle spectrum calculation broaden a couple of the distributions a little but do not change them radically. Marginalised 1d likelihood distributions of quantities such as sparticle masses (or mass differences) already show some significant structure from the data, providing interesting information for future

collider searches. In particular, the likelihood of the "golden cascade" at the LHC is peaked below 10 GeV , implying that stau reconstruction at hadron colliders is likely to be problematic at the LHC. Our likelihood distributions for $B_R(B_s \rightarrow \tau^+ \tau^-)$ corroborate the conclusions of ref. [32]: that current bounds upon the branching ratio do not yet place significant constraints upon m_{SUGRA} once other constraints have been taken into account, but any improvement on the upper bounds constrain the currently available parameter space. We have shown that the correlation between $B_R(B_s \rightarrow \tau^+ \tau^-)$ and $(g-2)_\mu$ noticed in Ref. [62] is much diluted once simultaneous variations of all m_{SUGRA} parameters are taken into account. The A^0 -pole annihilation region and the co-annihilation region each have approximately an order of magnitude more likelihood than the h^0 -pole region. We have chosen a range of parameters that is inconsistent with the focus point regime, which is excluded from our analysis. If one extended the upper bound of m_0 up to where the focus point resides, one would probably have to change the algorithm contained here in order to obtain its likelihood relative to the other dark matter annihilation regions. The reason for this is that the volume of parameter space would be too large compared to the typical width of the likelihood distribution in the 7d parameter space, implying that the MCMC would have to be run for an impractically large number of steps.

The analysis of Ref. [35] includes M_W and $\sin^2 \frac{1}{\text{eff}}$ in the t^2 statistic, excluding $M_{1=2} > 1500$ (600) GeV at the 90% confidence level for $m_t = 178$ GeV and $\tan \beta = 50$ (10) respectively. These numbers are not exactly reproduced in the present analysis for several reasons: we use a more up-to-date value of m_t , we vary $m_t, m_b, \tan \beta$ and M_Z simultaneously with the other SUGRA parameters and we do not include $M_W, \sin^2 \frac{1}{\text{eff}}$ in the t^2 . These two precision observables showed a preference for lower $M_{1=2}$ for $m_t = 178$ GeV. Having said that, the results are not wildly different, as an examination of Fig. 2a shows. An updated t^2 including the new combined Tevatron Run I/II top mass measurement [67] 172.9 ± 2.7 GeV will be used in a future revision of this paper. It will be interesting to see whether the light h^0 pole region survives LEP 2 Higgs mass constraints with the new top mass value, since m_{h^0} is heavily correlated to m_t .

We suspect that the MCMC techniques exemplified here could be found extremely useful in SUSY fitting programs such as FITTINO [68] and SFITTER [69] in order to provide a likelihood profile of the parameter space, including secondary local minima. These programs are designed to fit more general MSSM models than in SUGRA to data, with an associated increase in the number of free input parameters, so the linear calculating time of MCMCs ought to be very useful.

While our results presented for mSUGRA are in themselves interesting, it is obvious that the method will be applicable in a much wider range of circumstances. Once new observables become relevant, such as some LHC end-points, for example, it would be trivial to include them into the likelihood and re-perform the MCMC [70].

The method should be equally applicable to other models, and provided enough CPU power is to hand, could provide likelihood maps for models with even more parameters and/or detailed electroweak fits.

Acknowledgments

We would like to thank other members of the Cambridge SUSY Working Group, W de Boer, P Gondolo, P Haiger, B Heinemann, S Heinemeyer, A Peel and T Pfehn for helpful conversations. This work has been partially supported by PPARC.

A. Toy Models and Sampling

By definition, a sampler able to sample correctly from a pdf $p(x)$ must generate a list of x values whose local density, at large step-numbers, is proportional to the probability density $p(x)$ at each part of the space (in the preceding parts of the paper we have set this pdf to be the likelihood). The value of the constant of proportionality between the probability density and the local density of x values is unimportant, but the key point is that it is constant across the whole space.

It can sometimes be hard to implement a good sampler for a given probability distribution. In fact it is often easier to invent an algorithm which generates a sequence of x values, and which may superficially resemble a sampler, but which lacks constancy of proportionality over the space. We might call such algorithms pseudo-samplers as their output can sometimes resemble that of a true sampler, provided that the variation in proportionality is not too great across the space considered. Pseudo-samplers are sometimes useful (e.g. as a means of exploring a multidimensional space in which case sample density may be neither interesting nor the end product of the analysis).

In the present and in many other papers, however, sample density represents confidence in some particular part of parameter space, and is the final product of the analysis. Extreme care, then, must be taken to ensure that any creative modifications to established Markov Chain sampling techniques do not break the principle of detailed balance (the test which ensures that the algorithm remains a true sampler rather than a pseudo-sampler).

It is often desirable for Metropolis-Hastings type samplers to have an efficiency of about 25% for the acceptance of newly proposed points. Efficiencies much smaller than this may suggest that the proposal distribution is too wide and is too often proposing jumps to undesirable locations far away from the present point, leading to large statistical fluctuations in the result. Efficiencies much larger than this can be indicative of proposal distributions which are too narrow and may take too many steps to be practical to random-walk from one side of a region of high probability to the other. It is tempting, therefore, to adapt the present step size (i.e. proposal

distribution width) on the basis of recent efficiency. With a couple of toy examples, however, we will illustrate that this is a dangerous path to follow, and we will demonstrate that it breaks the principle of detailed balance, and thus turns the Markov Chain algorithm from a sampler into a pseudo-sampler.

We take as our example the method used by Baltz and Gondolo [37] which is designed to keep the target efficiency of the authors' Markov Chain close to 25% :

1. Double the current step size if the last three proposed points were all accepted
2. Halve the current step size if the last seven proposed points were all rejected.

We will refer to the above method as "the adaptive algorithm" and show that it fails to sample correctly from some simple distributions, a signature of detailed balance being broken.

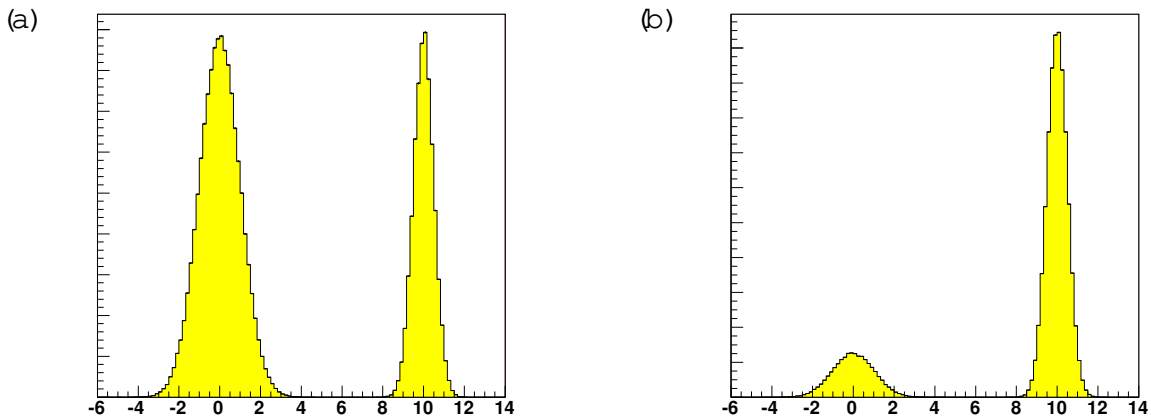


Figure 6: Binned samples of the double Gaussian distribution $p_{\text{double Gaussian}}(x)$. The normalization is arbitrary and has no relevance here. (a) uses a Metropolis-Hastings algorithm and yields a good approximation whereas (b) uses the adaptive algorithm.

Take, for example, the 1-dimensional double Gaussian probability distribution $p_{\text{double Gaussian}}(x)$ defined by

$$p_{\text{double Gaussian}}(x) = g(x; 0; 1) + g(x; 10; 1=2); \quad (\text{A.1})$$

where $g(x; m; \sigma) = \exp(-\frac{(x-m)^2}{2\sigma^2})$ is a Gaussian distribution of unit height and width centred on $x = m$. Note that the Gaussian near the origin is wider than the Gaussian near $x = 10$. This pdf breaks up the approximate situation along the $M_{1=2}$ direction in mSUGRA for large m_0 , as Fig. 2a shows. The narrow Gaussian would then correspond to the light h^0 -pole region, which is quite disconnected from the wider A^0 -pole region. A Metropolis-Hastings algorithm (see section 2) with a fixed Gaussian proposal pdf $Q(x)$ of width 5 was run for 2 000 000 steps and the

binned result is shown in Figure 6a. It reproduces the target distribution very well. In contrast, Figure 6b shows what happens when the adaptive algorithm is run on $p_{\text{DG au}}(x)$. Clearly the result is very different to that in Figure 6a and is thus very wrong. The narrow Gaussian has been sampled many times more frequently than it should have been relative to the wider one near the origin.

The adaptive algorithm ensures that whenever the current point is in one of the two Gaussian regions, the step size is adjusted to be proportional to the width of that region. This adaptation is not immediate (seven successive rejections must occur before the step size is halved) but suppose for the moment that adaptation were to take place almost immediately. For the moment, let us also neglect random fluctuations of the step size. In such a limit, when the current point is in the left-hand Gaussian region, the step size is double what it is when the current point is in the right-hand region. Making a proposal for a jump from the region on the left to the region on the right, therefore, is something like a 10-sigma event. In contrast, making the reverse proposal (from right to left) is more like a 20-sigma event. In this limit, it is thus $e^{(20)^2 - (10)^2} = e^{150}$ times more likely that jumps to the right get proposed than jumps to the left. This is a vast overestimate of the bias toward the narrow region for two reasons. Firstly, step size adaptation is not immediate (even when the step size is half of what it should be, quite a few steps occur before seven successive rejections). Secondly and more importantly, even when settled in one of the two regions, the adaptive step size makes excursions about its mean value. Excursions to very high step sizes (double or quadruple the average step size) are infrequent but still occur. When they do, they elevate the chance of proposing a jump from one region to another, and help to equilibrate between the two regions. Both of these effects reduce the bias favouring the narrow region, but still break detailed balance, and overall the right hand Gaussian is still sampled about 10 times more frequently than it should be.

For quite a different example, consider the truncated Cauchy distribution defined by

$$p_{\text{cauchy}}(x) / \begin{cases} 1/(1 + x^2) & \text{if } x > -500 \text{ and } x < 500; \\ 0 & \text{otherwise;} \end{cases} \quad (\text{A.2})$$

A faithful sampling from this distribution is shown in Figure 7(a), and a mis-sampling using the adaptive algorithm is shown for comparison in Figure 7(b). Although there is better correspondence between the samples generated by the two methods than was the case earlier, it is nevertheless evident that there are large differences between the degrees to which the two methods have sampled the tails of the distribution. As a consequence, samples from the adaptive method have a root-mean-squared value of 7.6 compared to the value of 17.9 obtained by the true sampling. The cause of the discrepancy is again due to the very different scales in the cauchy distribution.

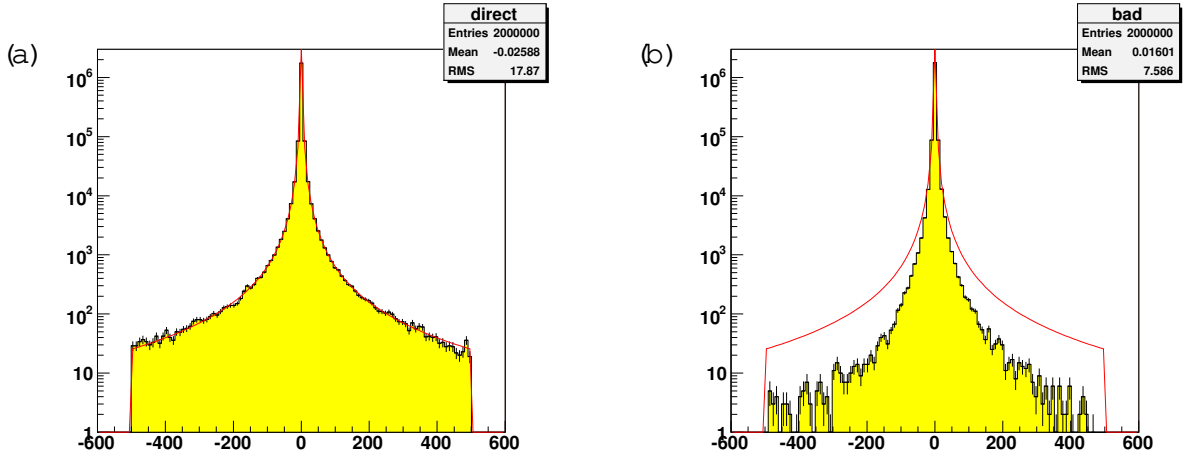


Figure 7: Binned sampling of a Cauchy distribution $1/(1+x^2)$ (shown in solid red line) truncated at $x = 500$. (a) shows the result of direct sampling and yields a good approximation whereas (b) uses the adaptive algorithm .

Its core is very narrow with a width of order 1, but there are significant parts of probability also lodged in the tails many orders of magnitude away. The adaptive method has to raise and lower the step size frequently to sample from the whole dynamical range, and in doing so it has to break detailed balance many times, resulting in the cumulative effect of an overall order of magnitude bias in the tails.

References

- [1] S.P. Martin, A supersymmetric primer, hep-ph/9709356.
- [2] J.R. Ellis, K.A. Olive, Y. Santoso, and V.C. Spanos, Gravitino dark matter in the CMSSM, Phys. Lett. B 588 (2004) 716, [hep-ph/0312262].
- [3] J.R. Ellis, J.S. Hagelin, D.V. Nanopoulos, K.A. Olive, and M. Srednicki, Supersymmetric relics from the big bang, Nucl. Phys. B 238 (1984) 453{476.
- [4] ATLAS Collaboration, W.W. Armstrong et. al., ATLAS: Technical proposal for a general-purpose pp experiment at the large hadron collider at cern, . CERN-LHCC-94-43.
- [5] D.N. Spergel et. al., First year Wilkinson Microwave Anisotropy Probe (WMAP) observations: Determination of cosmological parameters, Astrophys. J. Suppl. 148 (2003) 175, [astro-ph/0302209].
- [6] C.L. Bennett et. al., First year Wilkinson Microwave Anisotropy Probe (WMAP) observations: Preliminary maps and basic results, Astrophys. J. Suppl. 148 (2003) 1, [astro-ph/0302207].

[7] B .C .A llanach, G .B elanger, F .B oudjema, and A .P ukhov, Requirements on collider data to match the precision of WMAP on supersymmetric dark matter, JHEP 12 (2004) 020, [hep-ph/0410091].

[8] K .G riest and D .Seckel, Three exceptions in the calculation of relic abundances, Phys. Rev. D 43 (1991) 3191{3203.

[9] M .D rees and M .M .N ojiri, The neutralino relic density in minimal $N = 1$ supergravity, Phys. Rev. D 47 (1993) 376{408, [hep-ph/9207234].

[10] R .A mowitt and P .N ath, Cosmological constraints and SU (5) supergravity grand unification, Phys. Lett. B 299 (1993) 58{63, [hep-ph/9302317].

[11] A .D juadi, M .D rees, and J.-L .K neur, Neutralino dark matter in minimal SUGRA : Reopening the light higgs pole window, hep-ph/0504090.

[12] J .L .F eng, K .T .M atchev, and T .M oroi, Multi-Tev scalars are natural in minimal supergravity, Phys. Rev. Lett. 84 (2000) 2322{2325, [hep-ph/9908309].

[13] J .L .F eng, K .T .M atchev, and T .M oroi, Focus points and naturalness in supersymmetry, Phys. Rev. D 61 (2000) 075005, [hep-ph/9909334].

[14] J .L .F eng, K .T .M atchev, and F .W ilczek, Neutralino dark matter in focus point supersymmetry, Phys. Lett. B 482 (2000) 388{399, [hep-ph/0004043].

[15] M .B rhlik, D .J .H .C hung, and G .L .K ane, Weighing the universe with accelerators and detectors, Int. J. Mod. Phys. D 10 (2001) 367, [hep-ph/0005158].

[16] M .D rees et. al., Scrutinizing LSP dark matter at the LHC , Phys. Rev. D 63 (2001) 035008, [hep-ph/0007202].

[17] G .Polesello and D .R .T ovey, Constraining SUSY dark matter with the ATLAS detector at the LHC , JHEP 05 (2004) 071, [hep-ph/0403047].

[18] P .B ambade, M .B erggren, F .R ichard, and Z .Zhang, Experimental implications for a linear collider of the SUSY dark matter scenario, hep-ph/0406010.

[19] M .B attaglia et. al., Updated post-WMAP benchmarks for supersymmetry, Eur. Phys. J. C 33 (2004) 273{296, [hep-ph/0306219].

[20] B .C .A llanach, G .B elanger, F .B oudjema, A .P ukhov, and W .P orod, Uncertainties in relic density calculations in minimal SUGRA , hep-ph/0402161.

[21] T .M oroi, Y .S himizu, and A .Yotsuyanagi, Reconstructing dark matter density with e^+e^- linear collider in focus-point supersymmetry, hep-ph/0505252.

[22] J .L .B ourjaily and G .L .K ane, What is the cosmological significance of a discovery of wimps at colliders or in direct experiments?, hep-ph/0501262.

[23] L. Roszkowski, R. Ruiz de Austri, and T. Nishi, New cosmological and experimental constraints on the CM SSM, JHEP 08 (2001) 024, [hep-ph/0106334].

[24] H. Baer et. al., Updated constraints on the minimal supergravity model, JHEP 07 (2002) 050, [hep-ph/0205325].

[25] H. Baer, C. Balazs, and A. Belyaev, Neutralino relic density in minimal supergravity with co-annihilations, JHEP 03 (2002) 042, [hep-ph/0202076].

[26] H. Baer and C. Balazs, 2 analysis of the minimal supergravity model including WMAP, $g(\ell) \sim 2$ and b_1 constraints, JCAP 0305 (2003) 006, [hep-ph/0303114].

[27] J. R. Ellis, K. A. Olive, Y. Santoso, and V. C. Spanos, Supersymmetric dark matter in light of WMAP, Phys. Lett. B 565 (2003) 176{182, [hep-ph/0303043].

[28] U. Chattopadhyay, A. Corsetti, and P. Nath, WMAP constraints, SUSY dark matter and implications for the direct detection of SUSY, Phys. Rev. D 68 (2003) 035005, [hep-ph/0303201].

[29] A. B. Lahanas and D. V. Nanopoulos, WMAPing out supersymmetric dark matter and phenomenology, Phys. Lett. B 568 (2003) 55{62, [hep-ph/0303130].

[30] G. Belanger, F. Boudjema, A. Cottrant, A. Pukhov, and A. Semenov, Relic density of dark matter in SUSY and non-universal SUSY, hep-ph/0412309.

[31] CDF and D0 Collaboration, M. Headon, Searches for FCNC decays $b_s \rightarrow d_s \ell^+ \ell^-$, To appear in the proceedings of 32nd International Conference on High-Energy Physics (ICHEP 04), Beijing, China, 16-22 Aug 2004.

[32] J. R. Ellis, K. A. Olive, and V. C. Spanos, On the interpretation of $b_s \rightarrow d_s \ell^+ \ell^-$ in the CM SSM, hep-ph/0504196.

[33] S. Profumo and C. E. Yaguna, A statistical analysis of supersymmetric dark matter in the MSSM after WMAP, Phys. Rev. D 70 (2004) 095004, [hep-ph/0407036].

[34] J. R. Ellis, K. A. Olive, Y. Santoso, and V. C. Spanos, Likelihood analysis of the CM SSM parameter space, Phys. Rev. D 69 (2004) 095004, [hep-ph/0310356].

[35] J. R. Ellis, S. Heinemeyer, K. A. Olive, and G. Weiglein, Indirect sensitivities to the scale of supersymmetry, JHEP 02 (2005) 013, [hep-ph/0411218].

[36] L. S. Stark, P. Haider, A. Bialy, and F. Pauss, New allowed SUSY parameter space from variations of the trilinear scalar coupling A_0 , hep-ph/0502197.

[37] E. A. Baltz and P. Gondolo, Markov chain monte carlo exploration of minimal supergravity with implications for dark matter, JHEP 10 (2004) 052, [hep-ph/0407039].

[38] D. Mackay, Information Theory, Inference, and Learning Algorithms, Cambridge University Press, 2003.

[39] B .C .A llanach, D .G rellscheid, and F .Q uevedo, Genetic algorithms and experimental discrimination of SUSY models, *JHEP* 07 (2004) 069, [hep-ph/0406277].

[40] O .B rein, Adaptive scanning: A proposal how to scan theoretical predictions over a multi-dimensional parameter space efficiently, hep-ph/0407340.

[41] B .C .A llanach, J .P .J .H etherington, M .A .P arker, and B .R .W ebber, Naturalness reach of the Large Hadron Collider in minimal supergravity, *JHEP* 08 (2000) 017, [hep-ph/0005186].

[42] B .C .A llanach, Softsusy: A C++ program for calculating supersymmetric spectra, *Comput. Phys. Commun.* 143 (2002) 305{331, [hep-ph/0104145].

[43] S .E idemann et. al., Review of particle physics, *Phys. Lett. B* 592 (2004) 1{end.

[44] B .C .A llanach, A .D juadi, J .L .K neur, W .P orod, and P .Slavich, Precise determination of the neutral higgs boson masses in the MSSM, *JHEP* 09 (2004) 044, [hep-ph/0406166].

[45] A LEP H Collaboration, R .B arate et. al., Search for the Standard Model higgs boson at LEP, *Phys. Lett. B* 565 (2003) 61{75, [hep-ex/0306033].

[46] G .D egrassi, S .H einemeyer, W .H ollik, P .Slavich, and G .W eiglein, Towards high-precision predictions for the MSSM higgs sector, *Eur. Phys. J. C* 28 (2003) 133{143, [hep-ph/0212020].

[47] P .Skands et. al., SUSY Les Houches accord: Interfacing susy spectrum calculators, decay packages, and event generators, *JHEP* 07 (2004) 036, [hep-ph/0311123].

[48] G .B elanger, F .B oudjema, A .P ukhov, and A .S emenov, Micromegas: A program for calculating the relic density in the MSSM, *Comput. Phys. Commun.* 149 (2002) 103{120, [hep-ph/0112278].

[49] G .B elanger, F .B oudjema, A .P ukhov, and A .S emenov, Micromegas: Version 1.3, hep-ph/0405253.

[50] Muon g-2 Collaboration, G .W .B ennett et. al., Measurement of the negative muon anomalous magnetic moment to 0.7-ppm, *Phys. Rev. Lett.* 92 (2004) 161802, [hep-ex/0401008].

[51] M .P assera, The standard model prediction of the muon anomalous magnetic moment, *J. Phys. G* 31 (2005) R 75{R 94, [hep-ph/0411168].

[52] J .F .de Trooniz and F .J .Y ndurain, The hadronic contributions to the anomalous magnetic moment of the muon, *Phys. Rev. D* 71 (2005) 073008, [hep-ph/0402285].

[53] B .C .A llanach, A .B rignole, and L .E .Ibanez, Phenomenology of a mixed MSSM, *JHEP* 05 (2005) 030, [hep-ph/0502151].

[54] P. Gambino, U. Haisch, and M. Misiak, Determining the sign of the $b \bar{b}$ amplitude, *Phys. Rev. Lett.* **94** (2005) 061803, [hep-ph/0410155].

[55] Heavy Flavour Average Group Collaboration, <http://www.slac.stanford.edu/xorg/hfag>.

[56] The Tevatron Electroweak Working Group Collaboration, Combination of CDF and D0 results on the top-quark mass, hep-ex/0507006.

[57] A. Gelman and D. Rubin, Inference from iterative simulation using multiple sequences, *Stat. Sci.* **7** (1992) 457{472.

[58] CDF and D0 Collaboration, B. Heinemann, Search for MSSM higgs boson at CDF, talk at SUSY 2005, Durham, UK, 18-23 Jul 2005.

[59] M. M. Nojiri, K. Fujii, and T. Tsuchimatsu, Confronting the minimal supersymmetric standard model with the study of scalar leptons at future linear $e^+ e^-$ colliders, *Phys. Rev. D* **54** (1996) 6756{6776, [hep-ph/9606370].

[60] A. Dedes and B. T. Hutsman, Bounding the MSSM higgs sector from above with the Tevatron's $b_s \bar{b}_s \rightarrow \gamma \gamma$, *Phys. Lett. B* **600** (2004) 261{269, [hep-ph/0407285].

[61] CDF and D0 Collaboration, S. Dugad, Rare b -decays at tevatron, . To appear in the proceedings of the Hadron Collider Physics Symposium, Les Diablerets, Switzerland, 3-9 Jul 2005.

[62] A. Dedes, H. K. Dreiner, and U. Nierste, Correlation of $b_s \bar{b}_s \rightarrow \gamma \gamma$ and $(g-2)(\mu)$ in minimal supergravity, *Phys. Rev. Lett.* **87** (2001) 251804, [hep-ph/0108037].

[63] B. C. Allanach, C. G. Lester, M. A. Parker, and B. R. Webber, Measuring sparticle masses in non-universal string inspired models at the LHC, *JHEP* **09** (2000) 004, [hep-ph/0007009].

[64] LHC/LC Study Group Collaboration, G. Weiglein et. al., Physics interplay of the LHC and the ILC, hep-ph/0410364.

[65] B. C. Allanach, S. Kraml, and W. Porod, Theoretical uncertainties in sparticle mass predictions from computational tools, *JHEP* **03** (2003) 016, [hep-ph/0302102].

[66] G. Belanger, S. Kraml, and A. Pukhov, Comparison of SUSY spectrum calculations and impact on the relic density constraints from WMAP, hep-ph/0502079.

[67] The Tevatron Electroweak Working Group, Combination of CDF and D0 results on the top-quark mass, hep-ex/0507091.

[68] P. Bechtle, K. Desch, and P. W. Hennemann, Fittino, a program for determining MSSM parameters from collider observables using an iterative method, hep-ph/0412012.

[69] R. Lafaye, T. Pfehn, and D. Zerwas, Stter: Susy parameter analysis at LHC and LC, hep-ph/0404282.

[70] M. White, C. Lester, and A. Parker, Lost in space? Determining SUSY model parameters and masses at the LHC using cross sections, kinematic edges and other observables, to appear.